



**HAL**  
open science

## A comparison of indoor channel properties in V and E bands

Aliou Bamba, Francesco Mani, Raffaele d'Errico

► **To cite this version:**

Aliou Bamba, Francesco Mani, Raffaele d'Errico. A comparison of indoor channel properties in V and E bands. Antennas and Propagation (EUCAP), 2017 11th European Conference on, Mar 2017, Paris, France. pp.3361 - 3365, 10.23919/EuCAP.2017.7928448 . cea-01573428

**HAL Id: cea-01573428**

**<https://cea.hal.science/cea-01573428>**

Submitted on 9 Aug 2017

**HAL** is a multi-disciplinary open access archive for the deposit and dissemination of scientific research documents, whether they are published or not. The documents may come from teaching and research institutions in France or abroad, or from public or private research centers.

L'archive ouverte pluridisciplinaire **HAL**, est destinée au dépôt et à la diffusion de documents scientifiques de niveau recherche, publiés ou non, émanant des établissements d'enseignement et de recherche français ou étrangers, des laboratoires publics ou privés.

# A Comparison of Indoor Channel Properties in V and E Bands

Aliou Bamba<sup>\*,†</sup>, Francesco Mani<sup>\*,†</sup> and Raffaele D’Errico<sup>\*,†</sup>

<sup>\*</sup>CEA, LETI, Minatec Campus, 17 rue des Martyrs, 38054 Grenoble, France

<sup>†</sup>Université Grenoble-Alpes, Grenoble, France

**Abstract**—This paper presents wideband channel measurements in an office environment in the 62 GHz and 83 GHz frequency bands. Measurements were performed with a VNA and the mechanical steering of directive antennas at both the transmitter and receiver side, allowing a double-directional angular characterization. A comparison of propagation characteristics such as the path loss, multipaths clusters’ dispersion properties in the delay and angular domains are provided. Results show that similar propagation characteristics are attainable in the two bands considered.

## I. INTRODUCTION

The use of the classical frequency bands for mobile communications systems (i.e., 300 MHz-3 GHz) can not meet the requirements of future broadband communications, e.g., throughput, due to the congested and limited bandwidth therein. Nonetheless, the overwhelming demand of resources for broadband communications can be achieved by using the millimeter-wave (mmWave) spectrum where a large amount of bandwidth will enable multi-gigabit per second data transmission for the next generation of 5G wireless system [1]. Thus, regulation organisms such as the International Telecommunication Union-Radio Regulations (ITU-R) and the Federal Communications Commission (FCC) enable the use of several bands in the mmWave spectrum. These bands include - but not limited to - the unlicensed 60 GHz band (57-66 GHz, often referred to as *V-band*) and the licensed 70/80 GHz (71-76 GHz paired with 81-86 GHz, referred to as *E-band*). The broadband radio channel along with the propagation characteristics must be well understood in these bands for the standardization and design of future communications systems.

Several researches have addressed the indoor channels characteristics and models in the V-band [2], [3], as well as in the lower sub-band of the E-bands [3]–[5]. Measurements based statistical channel models for 60 GHz propagation in hospital environments are provided in [2]. A measurement-based spatio-temporal statistical channel model developed at 60 GHz and 70 GHz in several environments shows that identical channel model framework can be used to cover both frequencies [3]. Directional and omnidirectional path loss models and rms delay spread statistics have been investigated for co- and cross-polarized antennas configurations at 28 GHz and 73 GHz [5].

However, to the best of the author’s knowledge, only few researches have dealt with indoor channels measurements and characterisation in the upper band of the E-band. The

channel characterization results at 81-86 GHz in roof-to-street and street canyon scenarios are presented in [6], and [7] uses directional measurements in an indoor environment at 80.5-86.5 GHz to derive omnidirectional path loss model and dispersions properties of the channel.

In this paper, we investigate indoor mmWave channels at 59-65 GHz and 80.5-86.5 GHz through directive antennas measurements, and the propagation parameters are compared. The rest of the paper is organized as follows: the measurement campaigns, setup and scenarios are presented in Section II. The wideband channels are characterized in Section III and the measurement results and discussions are also provided. Finally, Section IV concludes the paper.

## II. CHANNEL MEASUREMENTS CAMPAIGN

### A. Measurement setup

A 4-port Vector Network Analyzer (VNA) has been used to record the two measurement campaigns. The first one was carried out at 59-65 GHz whereas the second was at 80.5-86.5 GHz. To be able to measure at these mmWave frequencies, two pairs of frequency converters - one for each band - have been employed at both sides of the transceivers. The VNA setup parameters for the measurement campaigns are presented in Table I. The low IF bandwidth permits us to have a noise floor of approximately -140 dB.

**TABLE I.** VNA setup and antennas directional parameters.

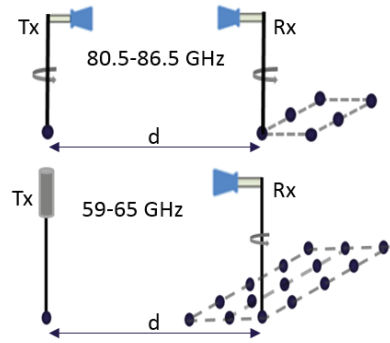
Frequencies	No. sweep points	IF bandwidth	Azimuth step (Tx, Rx)
59-65 GHz	2001	100 Hz	(360°, 10°)
80.5-86.5 GHz	2001	100 Hz	(45°, 10°)

For the 59-65 GHz measurements, we use a 0 dBi gain standard omni-directional antenna on the Tx side while we use a vertically polarized standard horn antenna with 20 dBi gain and approximately 20° half power bandwidth (HPBW) on the Rx side. For the 80.5-86.5 GHz measurements, a vertically polarized horn antenna with 10 dBi gain and a HPBW of 50° is used on the Tx side whereas a vertically polarized horn antenna with 20 dBi gain and a HPBW of 15° is utilized at the Rx (see Fig. 1(b)).

To fully investigate the channel in the azimuth domain, two positioner devices have been used to rotate the antennas and perform mechanical steering. Additionally, the rotating motor at Rx side is collocated with a 2D positioner that is able to scan in a grid of 80×80 cm<sup>2</sup>. A laptop operates the



(a) Measurement system in the office



(b) Scheme of the transceivers position.

Fig. 1. Measurement system (left) and transceivers position's scheme (right) in the office

VNA and the two positioner controllers through a Matlab software. Fig. 1(a) shows two pictures of the measurement environment with antennas connected to the converters and placed on the positioners. We consider one Tx location and four Rx locations. At each Rx location, the 2D positioner moved following a  $3 \times 5$  (resp.  $2 \times 3$ ) grid at 59-65 GHz (resp. 80.5-86.5 GHz) and the channel is probed at each position (see Figs. 1(b), 2).

### B. Measurement scenarios

The measurement campaign has been carried out at CEA-Leti. The scenario was a classical office of approximately  $50 \text{ m}^2$  with desks, storage cabinets and bookshelves (furniture was arranged at the sides of the room leaving a large empty part in the center where there was possible to perform the measurements). The room dimensions  $L$ ,  $l$ , and  $h$  are approximately 7 m, 7 m, and 2.6 m respectively. A floor plan of the office is depicted in Fig. 2, along with the locations of the transceivers.

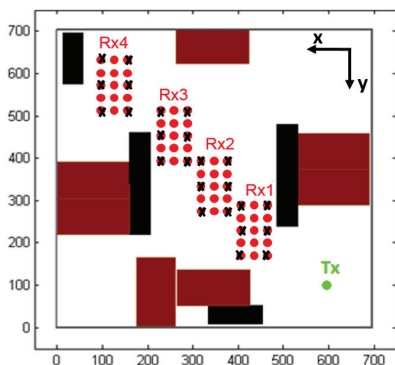


Fig. 2. Floor plan of the measurement environment and scenarios. At each location of the Rx, the red points (resp. black crosses) indicate the measurement positions at 59-65 GHz (resp. 80.5-86.5 GHz).

## III. CHARACTERIZATION OF MMWAVE WIDEBAND INDOOR CHANNELS AND MEASUREMENTS RESULTS

### A. Synthetization of directive channel measurements and omnidirectional power delay profile

At each pairing scanning direction of the Tx and Rx ( $\Omega_s^T$ ,  $\Omega_s^R$ ), the channel frequency response  $H_p(f, \Omega_s^T, \Omega_s^R)$  has been recorded and the corresponding channel impulse response (i.e.,  $h_p(\tau, \Omega_s^T, \Omega_s^R)$ ) computed. The power angular delay profile (PADP) of the channel is as follows:

$$PADP(\tau, \Omega_s^T, \Omega_s^R) = |h_p(\tau, \Omega_s^T, \Omega_s^R)|^2 \quad (1)$$

Note that (1) is further corrected to remove the gains introduced by the antennas. The synthetic omnidirectional PDP is then obtained as follows:

$$PDP_p(\tau) = \sum_{T=1}^{N_s^T} \sum_{R=1}^{N_s^R} PADP(\tau, \Omega_s^T, \Omega_s^R) \quad (2)$$

where  $N_s^T$  (resp.  $N_s^R$ ) is the number of scanning direction of the Tx (resp. Rx). Additional details on the synthetization procedure can be found in [3], [7].

The number ( $N_k$ ) of detectable paths and their corresponding delay  $\tau_k$ , ( $k = \{1 \dots N_k\}$ ) is determined from the synthetic PDP. Each delay  $\tau_k$  is mapped to a unique ( $\Omega_s^T$ ,  $\Omega_s^R$ ) couple defining the direction of departure and arrival of the  $k^{th}$  detected path. In the following, only the azimuthal direction is considered as the transceivers have the same height. The paths detection algorithm [3] is applied for paths identification. The algorithm searches for local maxima in the PDP by comparison with a threshold function [3].

Consider a path is found at  $\tau_k$ , the corresponding power is given by the following maximization function:

$$\alpha_k^2 = \max_{(\Phi_s^T, \Phi_s^R)} PADP(\tau_k, \Phi_s^T, \Phi_s^R) \quad (3)$$

where  $R = \{1 \dots N_s^R\}$  and  $T = \{1 \dots N_s^T\}$ . The (azimuth) angle of arrival (AoA) and departure (AoD) of the  $k^{th}$  path is given by the couple  $(\Phi_s^T, \Phi_s^R)$  maximizing (3).

Fig. 3 shows an example of omnidirectional PDP along with the detected multipaths. The two PDPs have been measured

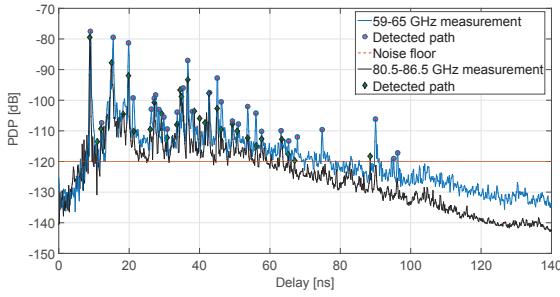


Fig. 3. Measured PDPs in the office (Rx1) and the detected specular paths.

- as best as possible - at the same position. We clearly see from Fig. 3 that *i*) the power level of multipaths is in general higher at 62 GHz than that at 83 GHz, and *ii*) the PDP drops faster in the noise floor at 83 GHz. These observations might be explained by the free space attenuation that is higher at higher frequencies.

### B. Path loss model

Path loss models are important features that provide informations such as coverage distance allowing efficient design of communications systems. The path gain value is obtained from the total relative received power  $P_t$  values, which in turns are obtained from the integration of the full PDP:

$$P_t = \frac{1}{PL} = \sum_{k=1}^K PDP(\tau_k), \quad (4)$$

where  $K$  is the number of sweep points. The path loss value, i.e.,  $PL$ , is then derived from the path gain. To model the path loss, we adopt the omnidirectional floating intercept model.

$$PL(d)[dB] = PL_0 + 10\hat{n} \log_{10} \left( \frac{d}{d_0} \right) + X_\sigma \quad (5)$$

where  $PL_0$  is the intercept in dB and  $\hat{n}$  is the path loss exponent that characterizes the increase in the channel path loss as a function of the Tx-Rx distance  $d$ . Both  $PL_0$  and  $\hat{n}$  are obtained from the intercept and slope of the best-fit to (5) according to the minimum mean square error (MMSE) criteria.  $PL(d)$  is the measured path loss at the distance  $d$  and is obtained from (4). Finally,  $X_\sigma$  represents the variation due to shadowing effects. Fig. 4 shows the path loss model at the two frequencies. We obtain  $\hat{n}$  (resp.  $PL_0$ ) of about 1.36 (resp. 67.88 dB) and 1.34 (resp. 69.58 dB) at 59-65 GHz and 80.5-86.5 GHz, respectively. Finally, we found that  $X_\sigma \sim \mathcal{N}(0, 0.66$  dB) at 63 GHz and  $X_\sigma \sim \mathcal{N}(0, 0.86$  dB) at 83 GHz.  $\mathcal{N}(\mu, \sigma)$  means a normal distribution with mean  $\mu$  and standard deviation  $\sigma$ .

### C. Delay dispersion properties

One of the important delay parameter - if not the most - is the root mean square delay spread ( $\tau_{rms}$ ) as it sets the bit error rate or the maximum achievable throughput of communication systems. The rms delay spread is the square root of the second central moment of the power delay profile.

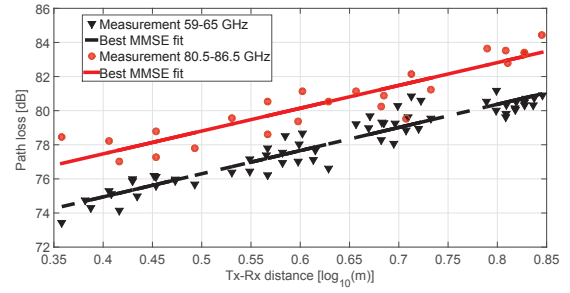


Fig. 4. Arrival and departure estimated angular spread.

After post processing, the  $\tau_{rms}$  values measured throughout the room vary from 4.60 ns to 8.40 ns for the first band (i.e., 59-65 GHz) while it ranges from 6.15 ns up to 11.5 ns for the 80.5-86.5 GHz band. We observe that there is clearly no trend between the  $\tau_{rms}$  values and the Tx-Rx distance. Therefore, the environment will be characterized by the mean rms delay spread, which are about 6.10 ns and 8.27 ns at 83.5 GHz and 62 GHz, respectively. Moreover, the  $\tau_{rms}$  values are randomly scattered around the mean values in both configurations. Hence, the actual rms delay spread of the environment can be thought of as the summation of a constant rms delay spread (i.e., the mean value), plus a random delay spread ( $X_\tau$ ) due to fading. From the measurements, we found that  $X_\tau \sim \mathcal{N}(0, 0.70$  ns) at 62 GHz and  $X_\tau \sim \mathcal{N}(0, 0.83$  ns) at 83 GHz.

### D. Clustering of the multipath

A cluster is a set of multipaths that have similar propagation characteristics in terms of delays and angles of arrival or departure... It has widely been proved that multipaths arrive in clusters mode in indoor environments [8]–[10]. Moreover, un-clustered models overestimate the channel capacity if the propagation paths are actually clustered [11]. Therefore, the clustering pattern of the multipaths and properties such as the dispersion properties are important for efficient design of future 5G communications systems. We group the estimated multipaths into clusters using the K-means algorithm [12] and the multipath component distance (MCD) is used as a metric to discriminate the clusters. Here we determine the MCD in the azimuth of arrival and delay domains.

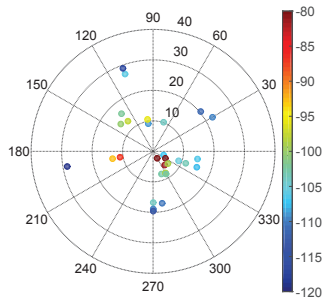
$$MCD_{AoA}^{ij} = \frac{1}{2} | \mathbf{a}_i - \mathbf{a}_j | \quad (6)$$

where  $\mathbf{a}_k = [\sin(\theta_k) \cos(\Phi_k), \cos(\theta_k) \cos(\Phi_k), \cos(\Phi_k)]^T$ .

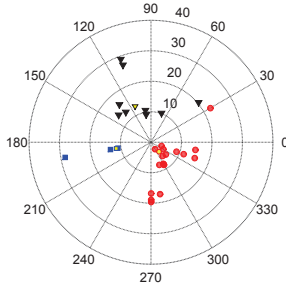
$$MCD_\tau^{ij} = \zeta \frac{|\tau_i - \tau_j| \tau_{std}}{\Delta\tau_{max}^2} \quad (7)$$

where  $\tau_{std}$  is the standard deviation of the delays,  $\Delta\tau_{max} = \max_{i,j} (|\tau_i - \tau_j|)$ , and  $\zeta$  is a suitable delay scaling factor fixing the importance of the delay domain. Here we set  $\zeta=1$ . The resulting metric to distinguish clusters is as follows:

$$MCD_{ij} = \sqrt{\| MCD_{AoA}^{ij} \|^2 + \| MCD_\tau^{ij} \|^2} \quad (8)$$

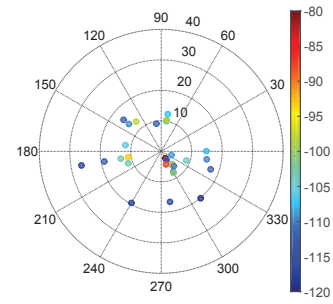


(a) Identified paths at 59-65 GHz

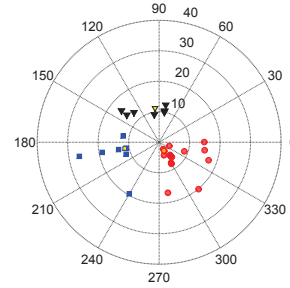


(b) Clustering at 59-65 GHz

Fig. 5. Identified paths and clustering pattern at Rx1-position 1.



(a) Identified paths at 80.5-86.5 GHz



(b) Clustering at 80.5-86.5 GHz

Fig. 6. Identified paths and clustering pattern at Rx1-position 1.

To avoid detection of insignificant clusters, the power of an identified cluster should be at least 1% of the total power. Figs. 5, 6 shows an example of detected paths and corresponding clusters. The red circles, blue square, and black triangle indicate the first, second, and third cluster, respectively. The yellow markers show the centroids. The concentric circles indicate the traveled distances - in meters - by the paths. We clearly assess three clusters in both bands. However, the number of cluster varies slightly throughout the office. The probability density function (PDF) of the number of identified cluster is shown in Fig. 7. On average, the number of cluster is similar for the two frequency bands. In general the number of cluster depends on the Rx location and the frequency as well. The most probable number of cluster is 2 at 80.5-86.5 GHz while it is 3 at 59-65 GHz. Moreover, we observe - for both bands - that 4 clusters mostly appear at the same location Rx4. The reason behind this may reside in Rx4 being near corner walls, closets and other furniture, as shown in Fig. 2, so there are multiple sources of scattering in different angular locations.

As comparison, [13] obtains a maximum of six clusters in a residential room at 60 GHz, [14] found up to four clusters in an outdoor micro-cell at 73 GHz, and 2 to 5 clusters are obtained for an indoor channel measurements at 28 GHz [15]. However, it is worth mentioning that the number of clusters will depend on the measurements dynamic range, the used algorithm to assess the multipaths, and so on. We now investigate the dispersion properties of the clusters

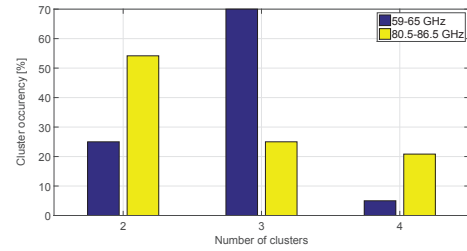


Fig. 7. Occurrence of the number of cluster

in the delay and angular domains. The general definition of rms angular spread [16] provides values from 0 to 1, and overcome the cyclicity of the angles when determining the directional spread. However, for small values of angular spread as expected for clusters, we adopt the definition of the rms angular spread [17]. We omit the formulas here for the sake of space. Table II displays the rms angular and delay spread values. For a Rx location, each parameter is calculated by averaging the values obtained from all the positions at that location.

We focus the analysis on the first cluster as it carries a significant part of the received power, i.e., at least 80% for Rx1, Rx2, Rx3 and 67% for Rx4. The rms angular and delay spread values of the first cluster are similar at both frequencies. The first cluster rms delay spread is quite constant over the Rx locations at the two frequencies. Namely, a mean rms delay spread of the first cluster of about 23.00 ns and 22.60 ns is obtained at 59-65 GHz and 80.5-86.5 GHz, respectively.

TABLE II. rms angular and delay spread values for both frequencies (bandwidth of 6 GHz). [-] indicates that the related cluster does not exist.

		1 <sup>st</sup> cluster		2 <sup>nd</sup> cluster		3 <sup>rd</sup> cluster		4 <sup>th</sup> cluster	
		$\bar{\sigma}_{\Phi}$ [°]	$\bar{\tau}_{rms}$ [ns]						
63 GHz	Rx1	37.10	24.20	20.45	19.30	20.20	20.50	[-]	[-]
	Rx2	22.35	21.60	13.70	12.40	12.60	16.70	[-]	[-]
	Rx3	18.45	22.30	19.10	12.95	8.30	14.80	4.30	27.90
	Rx4	12.20	23.90	11.40	23.20	9.40	9.40	2.50	9.05
83.5 GHz	Rx1	34	22.90	39.10	12.40	20.40	6.40	[-]	[-]
	Rx2	15.50	22	22.60	10.45	20.70	5.50	9.05	11.60
	Rx3	19.20	23.60	39.20	7.90	[-]	[-]	[-]	[-]
	Rx4	8.90	22	13.95	13.90	3.15	3.70	3.70	6.90

On the opposite, the rms angular spread varies along the Rx locations. The smallest (resp. highest) value occurs at Rx4 (resp. Rx1) location. Basically in Rx4 there are more clusters and so each of them is more colocated. We observe that the directional spread of clusters narrows when the receiver is located near reflectors and scatterers.

#### IV. CONCLUSION

A measurement campaign with directive antennas has been carried out in an office environment at two mmWave frequencies. Path loss model is evaluated, providing path loss exponents of 1.36 and 1.34 for measurements in 59-65 GHz and 80.5-86.5 GHz, respectively. We obtain two to four clusters at both frequencies and the number of clusters mostly depends on the transceivers location. The rms angular and delay spread of the most significant cluster have been determined. The first cluster rms angular spread ranges from 12.20° to 37.10° (resp. 8.90° to 34°) at 63 GHz (resp. 83.5 GHz) while its rms delay spread values are quite similar (i.e., ~ 23 ns) throughout the office at both frequencies. The office investigation shows that the large scale parameters variation is not significant at the two frequencies. Therefore, the same modelling framework is likely to be valid in both bands, at least in indoor environments.

#### ACKNOWLEDGMENT

The research leading to these results received funding from the European Commission H2020 programme under grant agreement 671650 (mmMagic Project).

#### REFERENCES

- [1] J. Wells. "Faster Than Fiber: The Future of Multi-Gb/s Wireless". *IEEE Microw. Mag.*, 10(3): pages 104–112, May 2009.
- [2] M. Kyrö, K. Haneda, J. Simola, K. Takizawa, H. Hagiwara, and P. Vainikainen. "Statistical Channel Models for 60 GHz Radio Propagation in Hospital Environments". *IEEE Trans. Antennas Propag.*, 60(3): pages 1569–1577, March 2012.
- [3] K. Haneda, J. Järveläinen, A. Karttunen, M. Kyrö, and J. Putkonen. "A Statistical Spatio-Temporal Radio Channel Model for Large Indoor Environments at 60 and 70 GHz". *IEEE Trans. Antennas Propag.*, 63(6): pages 2694–2704, June 2015.
- [4] S. Häfner, D. A. Dupleich, R. Müller, J. Luo, E. Schulz, C. Schneider, R. S. Thomä, X. Lu, and T. Wang. "Characterization of Channel Measurements at 70 GHz in Indoor Femtocells". In *IEEE 81st Vehicular Technology Conference*, pages pages 1–5, May 2015.
- [5] S. Deng, M. K. Samimi, T. S. Rappaport. "28 GHz and 73 GHz Millimeter-Wave Indoor Propagation Measurements and Path Loss Models". In *IEEE International Conference on Communications (ICC), ICC Workshops*, 2015.

- [6] M. Kyrö, S. Ranvier, V. M. Kolmonen, K. Haneda, and P. Vainikainen. "Long Range Wideband Channel Measurements at 81-86 GHz Frequency Range". In *4th European Conference on Antennas and Propagation (EUCAP)*, pages pages 1–5, Barcelona, April 2010.
- [7] A. Bamba, F. Mani, and R. D'Errico. "82-GHz Office Channel Measurements and Characterization". In *IEEE 20th International Symposium on Personal, Indoor and Mobile Radio Communications (PIMRC)*, Valencia, Spain, 4-7 September 2016.
- [8] A. A. M. Saleh, R. A. Valenzuela. "A Statistical Model for Indoor Multipath Propagation". *IEEE J. Sel. Areas Commun.*, SAC-5(2): pages 128–137, February 1987.
- [9] N. Czink, X. Yin, H. Özcelik, M. Herdin, E. Bonek, and B. H. Fleury. "Cluster Characteristics in a MIMO Indoor Propagation Environment". *IEEE Trans. Wireless Commun.*, 6(4): pages 1465–1475, April 2007.
- [10] F. Quintin, C. Oestges, F. Horlin, and P. De Doncker. "A Polarized Clustered Channel Model for Indoor Multiantenna Systems at 3.6 GHz". *IEEE Trans. Veh. Technol.*, 59(8): pages 3685–3693, October 2010.
- [11] K. H. Li, M. A. Ingram, and A. Van Nguyen. "Impact of Clustering in Statistical Indoor Propagation Models on Link Capacity". *IEEE Trans. Commun.*, 50(4): pages 521–523, April 2002.
- [12] N. Czink. "The Random Cluster Model - A Stochastic MIMO Channel Model for Broadband Wireless Communication Systems of the 3rd Generation and Beyond". PhD thesis, Technischen Universität Wien, 2007.
- [13] B. Neekzad, K. Sayrafian-Pour, J. S. Baras. "Clustering Characteristics of Millimeter Wave Indoor Channels". In *IEEE Wireless Communications and Networking Conference (WCNC)*, 31 March-3 April 2008.
- [14] M. R. Akdeniz, Y. Liu, M. K. Samimi, S. Sun, S. Rangan, T. S. Rappaport, and E. Erkip. "Millimeter Wave Channel Modeling and Cellular Capacity Evaluation". *IEEE J. Sel. Areas Commun.*, 32(6): pages 1164–1179, June 2014.
- [15] S. Hur, Y. J. Cho, J. Lee, N. G. Kang, J. Park, and H. Benn. "Synchronous Channel Sounder Using Horn Antenna and Indoor Measurements on 28 GHz". In *IEEE International Communications and Networking (BlackSeaCom)*, pages pages 83–87, 27-30 May 2014.
- [16] B. H. Fleury. "First- and Second-Order Characterization of direction Dispersion and space Selectivity in the Radio Channel". *IEEE Trans. Inf. Theory*, 46(6): pages 2027–2044, September 2000.
- [17] N. Czink, E. Bonek, X. Yin, and B. Fleury. "Cluster Angular Spreads in a MIMO Indoor Propagation Environment". In *IEEE 16th International Symposium on Personal, Indoor and Mobile Radio Communications (PIMRC)*, pages pages 664–668, Berlin, Germany, 11-14 September 2005.